Toroidal kinetic η_i-mode study in high-temperature plasmas

Cite as: Physics of Fluids B: Plasma Physics **4**, 1867 (1992); https://doi.org/10.1063/1.860040
Submitted: 22 November 1991 . Accepted: 25 March 1992 . Published Online: 04 June 1998

J. Q. Dong, W. Horton, and J. Y. Kim

Toroidal kinetic η_i-mode study in high-temperature plasmas

J. Q. Dong,[a] W. Horton, and J. Y. Kim
Institute for Fusion Studies, The University of Texas at Austin, Austin, Texas 78712

(Received 22 November 1991; accepted 25 March 1992)

A new kinetic integral equation for the study of the ion-temperature-gradient-driven mode in toroidal geometry is developed that includes the ion toroidal (curvature and magnetic gradient) drift motion ω_D, the mode coupling from finite $k_\parallel$ due to the toroidal feature of the sheared magnetic configuration. The integral equation allows the stability study for arbitrary $k_\parallel v_i/(\omega - \omega_D)$ and $k_\perp \rho_i$. A systematic parameter study is carried out for the low β circular flux surface equilibrium. Possible correlations between the unstable mode characteristics and some experimental results such as the fluctuation spectrum and the anomalous ion thermal transport measurements are discussed.

I. INTRODUCTION

The ion-temperature-gradient-driven mode (ITG mode), or η_i mode, has been of great interest in theoretical studies of plasma confinement physics and nuclear fusion in recent years. The objectives of these investigations are to understand and to explain some experimental observations, which indicate that the η_i-mode turbulence is a plausible candidate for the anomalous ion energy transport.[1–4] Some fluctuation studies[5,6] suggest the presence of the ion-mode feature, but a direct correlation of such turbulence with theory on the anomalous ion transport has not been obtained.

A comprehensive study[7] on the correlation between the η_i-mode turbulence and the density modification experiment on the tokamak fusion test reactor (TFTR[4]) tokamak is carried out, recently, with existing η_i-mode theories. It is pointed out[7] that present theories seem to be insufficient to explain some experimental observations, and a more complete study of the η_i mode is anticipated. Here an improved formalism for the most general integral equation for low-frequency perturbations such as the η_i mode in toroidal geometry derived in Ref. 8 is developed and applied to obtain detailed numerical results for tokamak plasma parameters.

Theoretical studies on the η_i mode are numerous. Most of the studies, however, are performed under some limits or approximations. The slab η_i-mode studies[9–11] only consider the driving force due to the coupling of the parallel transit of the particles with the temperature gradient. The kinetic effects, including the arbitrary Larmor radius effect and the full parallel Landau resonance damping, are taken into account, while the particle drift motion due to magnetic curvature and gradient is neglected. In the fluid limit[12–14] these kinetic effects are neglected, where some nonlinear studies are carried out due to the simplicity of the equations used. Local toroidal η_i-mode studies[15,16] consider the driving force due to the coupling of the particle curvature and grad-B drift with temperature gradient, while neglecting the variation of the drift motion along the poloidal direction and shear effect. Some expansions,[17,18] such as small $k_\parallel v_i/(\omega - \omega_D)$, can significantly reduce the complexity of the gyrokinetic equation in toroidal geometry, but are not appropriate when such conditions are broken. An integral equation, including all ion kinetic mechanisms except the trapped particle effect, is derived in Ref. 8, but emphasis is put on the fluid and local kinetic limits and very few results are available in the general kinetic parameter regime. A comprehensive study of the η_i mode is carried out in Ref. 19 using a particle simulation approach.

A more complete study of the η_i mode in toroidal geometry is needed, either in order to more accurately assess the actual relevance of the η_i mode to the experimental observations or for the completeness of the η_i-mode theoretical study.

In the present work we derive a new integral equation to study the ion-temperature-gradient-driven mode in toroidal geometry. This equation includes the curvature and magnetic gradient drift motion of the ions and the mode coupling due to the spatial inhomogeneity in the toroidal magnetic configuration. The full ion transit $k_\parallel v_\parallel$ and toroidal drift effects $\omega_D(v_\perp^2, v_\parallel^2, \theta)$ are retained while the ion bouncing motion is neglected for simplicity. Electrons are considered to be adiabatic. Essentially, the new equation is equivalent to the one derived in Ref. 8. Nevertheless, the integral equation given in the present work has some characteristics that allow the fast computation of the spectrum of eigenvalues with the modest computer time (3 min/eigenvalue on the CRAY-2). By using the integral equation, detailed full kinetic results for a number of issues, such as the effects of toroidicity, safety factor, shear, and the ratio of the electron temperature to the ion temperature on the mode are obtained. At the same time a quasitoroidal model is considered, where the magnetic curvature and grad-B drift is assumed to be constant over a flux surface (a more detailed explanation is given in Sec. II). Results from the general toroidal equation, the quasitoroidal model, and the familiar local kinetic equation are compared.

It should be noted that attention is focused on the ion dynamics and electrons are considered to be adiabatic in this work. In addition, the usual equilibrium model with

[a] Permanent address: Southwestern Institute of Physics, Leshan, People's Republic of China.

 0899-8213/92/071867-10$04.00

circular flux surfaces has been used. The electron dynamics such as trapped electron effects and noncircular flux surface configurations are beyond the scope of present work, but are studied by Rewoldt and Tang[20] with a different approach. Rewoldt and Tang[20] show that the trapped electron effects on the η_i mode are significant when η_i approaches the threshold value ($\eta_i \sim 1$) obtained here with the adiabatic electron response (Fig. 11). When the trapped electrons destabilize the mode the direction of the mode rotation changes to the electron diamagnetic direction.

The remainder of this work is organized as follows. In Sec. II the new integral equation is given and its characteristics are discussed. The numerical results are presented and compared in Sec. III, and the concluding remarks and discussions are given in Sec. IV.

II. INTEGRAL EQUATION IN TOROIDAL GEOMETRY

The dynamics of a low-frequency electrostatic perturbation in inhomogeneous plasmas is described by the quasineutrality condition

$$\tilde{n}_e=\tilde{n}_i . \tag{1}$$

Here, in the η_i-mode study the perturbed electron density $\tilde{n}_e$ is taken to be the adiabatic response to the electrostatic perturbation $\tilde{\phi}$; i.e.,

$$\tilde{n}_e=(en_{0e}/T_e)\tilde{\phi} . \tag{2}$$

On the other hand, the perturbed ion density $\tilde{n}_i$ in an axisymmetric toroidal geometry (like a tokamak) is given by

$$\tilde{n}_i=-\frac{en_{0i}}{T_i}\tilde{\phi}+\int d^3v\, J_0(\alpha)h, \tag{3}$$

where T_e and T_i are the temperature of the electrons and the ions, respectively, and $\alpha = (2b_i)^{1/2}v_\perp$, $v = v/v_{ti}$, $2b_i = k_\perp^2 v_{ti}^2/\Omega_i^2$, $v_{ti} = (2T_i/m_i)^{1/2}$, and $\Omega_i = eB/m_ic$ is the ion gyrofrequency, $J_0(\alpha)$ the Bessel function of zeroth order. The nonadiabatic response h is determined by solving the gyrokinetic equation,

$$i\frac{v_\parallel}{Rq}\frac{\partial}{\partial\theta}h+(\omega-\omega_D)h = (\omega-\omega_{*T})J_0(\alpha)F_M\frac{en_{0i}}{T_i}\hat{\phi}(\theta), \tag{4}$$

with

$$\omega_D=2\tau_e^{-1}\epsilon_n\omega_{*e}(\cos\theta+\hat{s}\theta\sin\theta)\left(\frac{v_\perp^2}{2}+v_\parallel^2\right), \tag{5}$$

where $\omega_{*T} = -\tau_e^{-1}\omega_{*e}[1 + \eta_i(v_\perp^2 + v_\parallel^2 - \frac{3}{2})]$, $\omega_{*e} = (ck_\theta T_e)/eBL_n$ is the electron diamagnetic drift frequency, $L_n = -(d\ln n/dr)^{-1}$ is the density gradient scale length; $\eta_i = L_n/L_{Ti}$, with L_{Ti} being the ion temperature gradient scale length; $\epsilon_n = (L_n/R)$, with R being the major radius of the torus; $\tau_e = T_e/T_i$; the magnetic shear $\hat{s} = (r/q)(dq/dr)$, with q being the safety factor; and $F_M = (\pi v_{ti}^2)^{-3/2}\exp(-v^2)$. We note that the well-known ballooning mode representation,[21]

$$\tilde{f}_n(r,\theta,\zeta)=\sum_{m=-\infty}^{\infty}e^{im\theta}\int_{-\infty}^{\infty}e^{-im\theta'} \times e^{-in(\zeta-q\theta')-i\omega t}\tilde{f}_n(\theta')d\theta', \tag{6}$$

where ζ and θ are the toroidal and the extended poloidal angles, respectively, has been used in deriving Eq. (4), and the usual circular flux surface equilibrium model has been used in Eq. (5).

In solving Eq. (4), for simplicity, we ignore the trapped ion contribution, which is relevant only for very low-frequency perturbations of $\omega \simeq \omega_{bi}$ (ion bounce frequency). In addition, for the passing particles we neglect the $v_\parallel$ modulation along the unperturbed particle orbit due to the equilibrium magnetic field. The following Fredholm homogeneous integral equation of the second kind[23] can be obtained from the quasineutrality condition Eq. (1),

$$(1+\tau_e)\hat{\phi}(\theta)=\int_{-\infty}^{+\infty}d\theta'\,K(\theta,\theta')\hat{\phi}(\theta'), \tag{7}$$

with

$$K(\theta,\theta')=-i\tau_e\int_0^\infty 2\pi v_\perp\,dv_\perp \times\int_0^\infty dv_\parallel\frac{qR}{|v_\parallel|}e^{i[\sigma(\theta)-\sigma(\theta')]\mathrm{sgn}(\theta-\theta')} \times(\omega-\omega_{*T})J_0(\alpha)J_0(\alpha')F_M, \tag{8}$$

where

$$\sigma(\theta)=\int^\theta d\theta''\frac{qR}{|v_\parallel|}[\omega-\omega_D(\theta'')], \tag{9}$$

and the nonadiabatic response h, the solution of Eq. (4) with the boundary condition $h(\theta)=0$ as $|\theta|\to\infty$,[8] has been obtained and substituted into Eq. (3). The $v_\perp$ integration in Eq. (8) can be performed analytically, and the resulting equation is Eq. (7) of Ref. 8.

A. Toroidal kinetic integral equation

In contrast to Ref. 8, the $v_\parallel$ integration in Eq. (8) is changed to the integration over τ by introducing

$$\tau=\frac{qR|\theta-\theta'|}{v_\parallel v_{ti}} . \tag{10}$$

It is easy to recognize that τ is the time interval $t-t'$, with t and t' being the time corresponding to the extended poloidal positions θ and θ', respectively, in the present case that the modulation of $v_\parallel$ along unperturbed particle orbit is neglected. Now it is the right time to point out that the kernel of the integral equation is the ensemble average over the Maxwellian velocity of the two-time $t-t'=\tau$ correlation function required for the nonlocal plasma susceptibility operator $\hat{\chi}_j$ defined by $\delta n_j(x,t) = (n_0e_j/T_j)\hat{\chi}_j\tilde{\phi}(x',t')$. The integration over $v_\perp$ in Eq. (8) is carried out by taking advantage of the collisionless phase mixing that occurs from the velocity dispersion in the grad-B drift and the result gives the power law decay in τ of the integral operator. Thus for large $\omega_D\tau$, corresponding to small ω/ω_D, the correlation function decays as

$1/(\tau\omega_D)^{3/2}$ [see Eq. (12) below], even for $k_\parallel = 0$, where the usual transit time phase mixing $\exp(-k_\parallel^2 v_T^2 \tau^2)$ vanishes. For small τ the expansion of Eq. (7) leads to the usual small ω_D/ω fluid regime. We also use the dimensionless variable $k = \hat{s}(r_0)k_\theta\theta = \hat{s}(r_0)(m/r_0)\theta$, which is the Fourier transform of the radial variable $x = r - r_0$ [r_0 being defined by $q(r_0) = m/n$] in the toroidal model given by Eq. (6). The connection between $k = k_x\rho_s$ and the ballooning variable θ is derived by expanding the phase factor $\exp[inq(r)\theta']$ in Eq. (6) about the local nearest rational surface. By introducing such conversion from θ's to k's, the integral equations (7) and (8) now can be written as

$$(1+\tau_e)\hat{\phi}(k) = \int_{-\infty}^{+\infty} \frac{dk'}{\sqrt{2\pi}} K(k,k')\hat{\phi}(k'), \tag{11}$$

with

$$K(k,k') = -i\int_{-\infty}^{0} \omega_{*e}\, d\tau \frac{\sqrt{2}e^{-i\omega\tau}}{\sqrt{a}(1+a)\sqrt{\lambda}} \times e^{-(k-k')^2/4\lambda}\left[\frac{\omega}{\omega_{*e}}\tau_e + 1 - \frac{3}{2}\eta_i + \frac{2\eta_i}{(1+a)} \times\left(1 - \frac{k_\perp^2 + k_\perp'^2}{2(1+a)\tau_e} + \frac{k_\perp k_\perp'}{(1+a)\tau_e}\frac{I_1}{I_0}\right) + \frac{\eta_i(k-k')^2}{4a\lambda}\right]\Gamma_0(k_\perp, k_\perp'), \tag{12}$$

where

$$\lambda = \frac{\tau^2}{\tau_e a}\left(\frac{\hat{s}}{q}\epsilon_n\right)^2 \omega_{*e}^2, \tag{13}$$

$$a = 1 + \frac{i2\epsilon_n}{\tau_e}\omega_{*e}\tau \times\left(\frac{[(\hat{s}+1)(\sin\theta - \sin\theta') - \hat{s}(\theta\cos\theta - \theta'\cos\theta')]}{(\theta-\theta')}\right), \tag{14}$$

$$\theta = \frac{k}{\hat{s}k_\theta}, \quad \theta' = \frac{k'}{\hat{s}k_\theta}, \tag{15}$$

$$\Gamma_0 = I_0\left(\frac{k_\perp k_\perp'}{\tau_e(1+a)}\right)e^{-(k_\perp^2 + k_\perp'^2)/2\tau_e(1+a)}, \tag{16}$$

$$k_\perp^2 = k_\theta^2 + k^2, \quad k_\perp'^2 = k_\theta^2 + k'^2, \tag{17}$$

and $I_j (j = 0,1)$ is the modified Bessel function of order j. Also, the wave numbers k_θ, k, and k' are normalized to ρ_s^{-1} with $\rho_s = \sqrt{2T_e/m_i}/\Omega_i$.

B. Quasitoroidal kinetic integral equation

By looking at Eqs. (5) and (14) it is easy to notice that the nonlocal contribution of $\omega_D(\theta)$ in Eq. (5) ($\cos\theta + \hat{s}\theta\sin\theta$), appears in the second term of Eq. (14) on the right side as the average of ω_D [Eq. (5)] over the region (θ',θ). If we choose $\theta = 0$ in Eq. (5), which means that the magnetic curvature and grad-B drifts are considered to be constant and equal to the maximum value at $\theta = 0$, then we obtain the following integral equation for the quasitoroidal model,[24]

$$(1+\tau_e)\hat{\phi}(k) = \int_{-\infty}^{+\infty} \frac{dk'}{\sqrt{2\pi}} K(k,k')\hat{\phi}(k'), \tag{18}$$

with

$$K(k,k') = -i\int_{-\infty}^{0} \omega_{*e}\, d\tau \frac{\sqrt{2}e^{-i\omega\tau}}{\sqrt{a}(1+a)\sqrt{\lambda}} e^{-(k-k')^2/4\lambda} \times\left[\frac{\omega}{\omega_{*e}}\tau_e + 1 - \frac{3}{2}\eta_i + \frac{2\eta_i}{(1+a)} \times\left(1 - \frac{k_\perp^2 + k_\perp'^2}{2(1+a)\tau_e} + \frac{k_\perp k_\perp'}{(1+a)\tau_e}\frac{I_1}{I_0}\right) + \frac{\eta_i(k-k')^2}{4a\lambda}\right]\Gamma_0(k_\perp, k_\perp'), \tag{19}$$

where

$$\lambda = \frac{\tau^2}{\tau_e a}\left(\frac{L_n}{L_s}\right)^2 \omega_{*e}^2, \tag{20}$$

$$a = 1 + \frac{i2\epsilon_n}{\tau_e}\omega_{*e}\tau, \tag{21}$$

and L_s is the scale length of the magnetic shear. All remaining expressions are the same as in the toroidal kinetic integration case. If we put $\epsilon_n = 0$ in Eq. (18), then it reduces to the sheared slab η_i mode integral equation.[10] On the other hand, if $\hat{\phi}(k) = \text{const}$, corresponding to $\tilde{\phi}(x) \sim \delta(x-x')$, then the k' integration can be done and Eq. (18) reduces to the local kinetic dispersion relation.[16]

Essentially, Eq. (11) is equivalent to Eq. (5) of Ref. 8 (this will be referred to as the Romanelli equation hereafter). However, Eq. (11) has some characteristics compared with the Romanelli equation.

First, Eq. (11) shows more clearly the relation between the sheared slab and the toroidal modes. This is due to the change of the ballooning mode space variable θ to k, which corresponds to the Fourier transform of the real space variable x in the sheared slab limit. In addition, in Eq. (11) it is easy to identify the shear effect and ballooning effect, which are both considered to be important in toroidal geometry. In a general toroidal geometry, where the eigenvalue equation is a complicated two-dimensional equation in the (r,θ) space, we may consider that $k_\parallel$ decomposes into $k_\parallel = k_\parallel^{(t)} + k_\parallel^{(s)}$, where $k_\parallel^{(t)}$ and $k_\parallel^{(s)}$ stand for the ballooning contribution to $k_\parallel$ (from the variation of the poloidal modulation in the θ direction of the equilibrium) and magnetic shear contribution to $k_\parallel$ (from the variation of the direction of the magnetic field with r), respectively. In the well-known ballooning mode formalism for the toroidal mode, the shear effect $k_\parallel^{(s)}$ is obtained from the twisting of the eikonal phase factor in Eq. (6), which locally varies as $e^{inq'\theta x}$ for the radial profile of the eigenfunction to reduce the two-dimensional problem to a one-dimensional problem. Effectively, with this local expansion the ballooning mode formalism emphasizes the exact treatment of the

ballooning structure of the eigenfunction and the toroidal curvature and the magnetic gradient drifts, i.e., the ballooning effect, while admits a poor treatment of the local shear and the global radial structure of the eigenmode. To treat the local shear effect and the global structure of the mode more exactly, an alternative approximate method has, recently, been used in the fluid simulation study by Hong and Horton.[24] This method[24] assumes that the toroidal driving force is a constant over a flux surface without variation along the poloidal angle θ, so that $k_{\parallel}^{(t)} \simeq 0$. The toroidal driving force is taken to be the local maximum value at the point $\theta=0$, so that $\omega_D \simeq k_y v_D = 2\epsilon_n \omega_* (v_\perp^2/2 + v_\parallel^2)$. While this model[24] makes it possible to do the nonlinear simulation of the toroidal mode, we show here that in the long-wavelength regime $k_\theta \rho_s \sim \epsilon_n/q$, it overestimates the growth rate by a factor of 2.

In the quasitoroidal model [Eq. (18)] the same approach as in Ref. 24 is used for the kinetic study of the η_i mode. In this model the eigenvalue equation takes the same form as the sheared slab model, except the toroidal mode driving force, which is assumed to be uniform over a flux surface, has been included. So that this model emphasizes the shear effect and ignores the ballooning effect, while both approaches keep the toroidicity induced drift effect, which is the most important driving force in toroidal geometry.

The second difference of our equation from the Romanelli equation is that the numerical calculation of the eigenvalue can be performed more efficiently than using the Romanelli equation. This is because, first, the kernel $K(k,k')$ of Eq. (11), as given in Eq. (12), vanishes as $e^{-(k-k')^2}$ when $(k-k')$ increases, while the kernel of Romanelli equation vanishes as $e^{-(\chi-\chi')}$ when $(\chi-\chi')$ increases [χ in the Romanelli equation is the extended poloidal angle as θ in Eq. (11)]. Second, the kernel of the Romanelli equation oscillates very rapidly due to the large phase factor in Eq. (8), $\sigma(\theta)-\sigma(\theta')$, when $v_\parallel \to 0$ and $(\chi-\chi')$ is small, but not zero. The oscillation characteristics of the kernel in Eq. (11) do not change when $\tau \to 0$ and $(k-k')$ is small but not zero. Here, by changing the $v_\parallel$ integration to τ integral the phase mixing of the oscillation is taken into account analytically, leaving the rapid convergent kernel. It is these differences that make the matrix obtained from Eq. (11) a more nearly diagonal matrix, which improves the numerical representation of the integral operator and allows the eigenvalue problem to converge much faster. Our numerical experience has shown that the computer time needed to study toroidal η_i mode with Eq. (11) is about half that required for the Romanelli equation.

Finally, the local kinetic dispersion relation,[16]

$$1+\frac{1}{\tau_e}=\int d^3v \frac{(\omega-\omega_{*T})J_0^2(\alpha)F_M}{\omega-\omega_D-k_\parallel v_\parallel}, \tag{22}$$

can be easily obtained from Eq. (4) by taking $(1/Rq)\times(\partial/\partial\theta) = ik_\parallel$ and $\omega_D(\theta) = \omega_D(0)$. Equation (22) also follows from Eq. (18) by taking $\phi(k)=$const, and doing the k' integral.

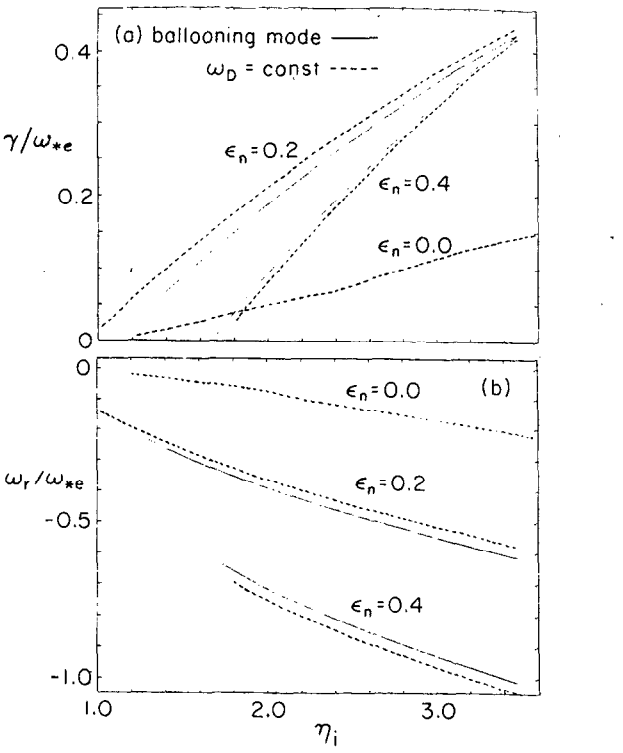

FIG. 1. (a) Normalized growth rate γ/ω_{*e} and (b) real frequency ω_r/ω_{*e} vs η_i for $T_e/T_i = 1$, $k_\theta\rho_s = 0.75$, $L_n/L_s = 0.1$, and $\epsilon_n = 0.2$ and 0.4. The solid lines are the general toroidal with $q=2$, and $\hat{s} = L_n q/L_s\epsilon_n$, and the dotted lines are the quasitoroidal approximation and sheared slab limit with $\epsilon_n = 0$.

III. NUMERICAL RESULTS

A computer code is developed to solve Eq. (11) numerically. At $k=k'$ the kernel has a logarithmic singularity that can be easily handled by standard techniques, as pointed out in Ref. 8. The integration over τ in Eq. (12) is performed with a Gaussian rule of even order. The integration over k' in Eq. (11) is carried out with a rectangle rule, except near $k'=k$, where the Gaussian rule of even order is used.

The computer code is tested in two ways. First, it is run in the sheared slab limit ($\epsilon_n = 0$) and tested with the results given in Ref. 10. Second, for $\eta_i = 2.5$, $\hat{s}=q=\tau=1$, $k_\theta\rho_s = 0.45$, $\epsilon_n = 0.25$ the normalized real frequency $\Omega_r = \omega_r/\omega_{*e} = -0.607$, and the growth rate $\Omega_i = \gamma/\omega_{*e} = 0.258$ are obtained for the toroidal mode. The growth rate agrees well with the result given in Ref. 8 while the real frequency is not available there.

In general, the dimensionless complex eigenvalue Ω is a function of the six parameters η_i, ϵ_n, τ, $\hat{s}$, q, and k_θ. We have recorded and tabulated the Ω's from all cases that we have run in a database to be made available in a NERSC (National Energy Research Supercomputer Center) public domain file.

A. η_i and $k_\theta\rho_s$ variation

The normalized growth rate and real frequency as a function of η_i are given in Fig. 1 for $T_e/T_i = 1$, $k_\theta\rho_s$

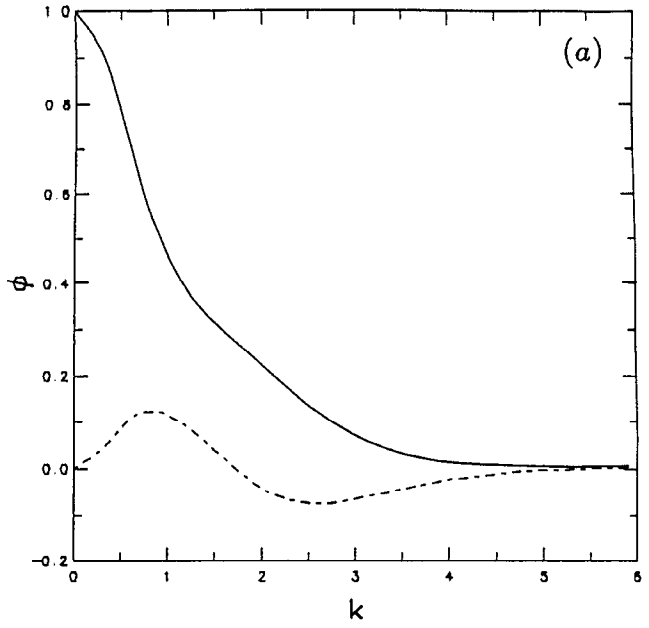

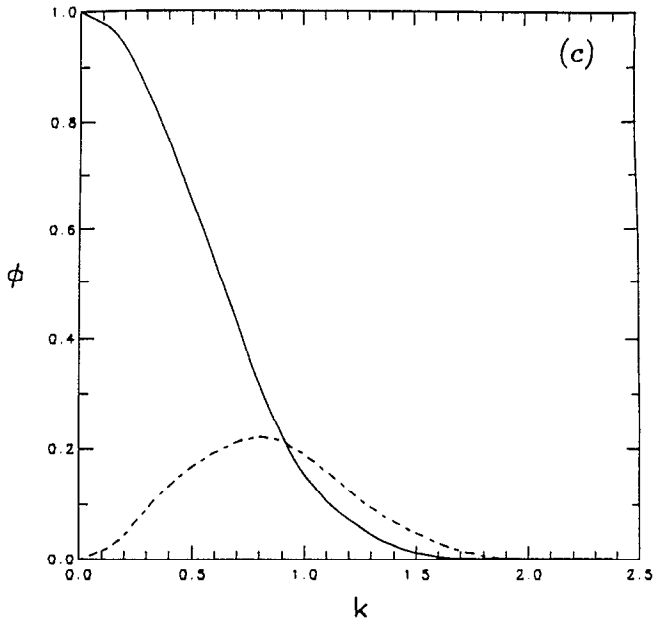

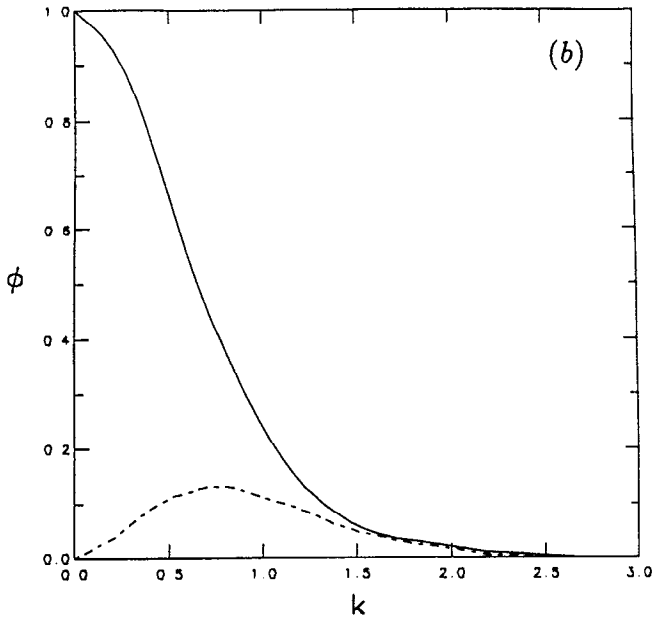

FIG. 2. Eigenfunctions $\hat{\phi}(k)$ in the k space for the three cases of Fig. 1 with $\eta_i = 3.0$; (a) the sheared slab mode; (b) the quasitoroidal model with $\epsilon_n = 0.2$; and (c) the general toroidal model with $\hat{s}=1.0$ and $q=2.0$. The other parameters are the same as used in Fig. 1. The solid lines are the real part and the dotted lines the imaginary part.

$= 0.75$, $L_n/L_s = 0.1$, and $\epsilon_n = 0.2$. The solid lines are from Eq. (11) of the ballooning formalism and the dotted lines are the results from Eq. (18) of the quasitoroidal model. The parameters $\hat{s}$ and q for Eq. (11) are chosen, such that $L_n/L_s = \hat{s}\epsilon_n/q = 0.1$ ($q=2$, $\hat{s}=1$). As a comparison, the results for a slab with the same parameters are given in Fig. 1 by the $\epsilon_n = 0$ curves. For $\epsilon_n = 0.2$ and 0.4, we find that there is a good agreement between full Eq. (11) and the quasitoroidal model in the growth rate and the real frequency.

In Fig. 2 we show the eigenfunctions in the k space obtained from the three models given in Fig. 1 with $\eta_i = 3.0$ and $T_e/T_i = 1.0$. Figure 2(a) is the eigenfunction $\hat{\phi}(k)$ in a sheared slab for $L_n/L_s = 0.1$ and $k_y\rho_s = k_\theta\rho_s = 0.75$. Figure 2(b) is the eigenfunction in the quasitoroidal model with $\epsilon_n = 0.2$ while the other parameters are the same as that in the slab case. The eigenfunction from Eq. (11) is shown in Fig. 2(c) with $\hat{s}=1.0$, $q=2.0$, and the same parameters used by the other models. The solid lines are the real part and the dotted lines the imaginary part. Here, we note that the eigenfunctions in the quasitoroidal and sheared slab models are just the Fourier transform of the real $x$space eigenfunction. The eigenfunctions in Figs. 2(b) and 2(c) are very similar to each other with a half-width about $0.6\rho_s^{-1}$, while the meaning of this is different in each case. The half-width of the eigenfunction in the sheared slab case is about $1\rho_s^{-1}$, which means that the slab mode has a shorter wavelength than the quasitoroidal mode in real x space. So that the toroidal effect can significantly increase the transport induced by the η_i-mode turbulence when estimated with the mixing length theory, as given in Refs. 7 and 24.

The growth rate and real frequency versus $k_\theta\rho_s$ are

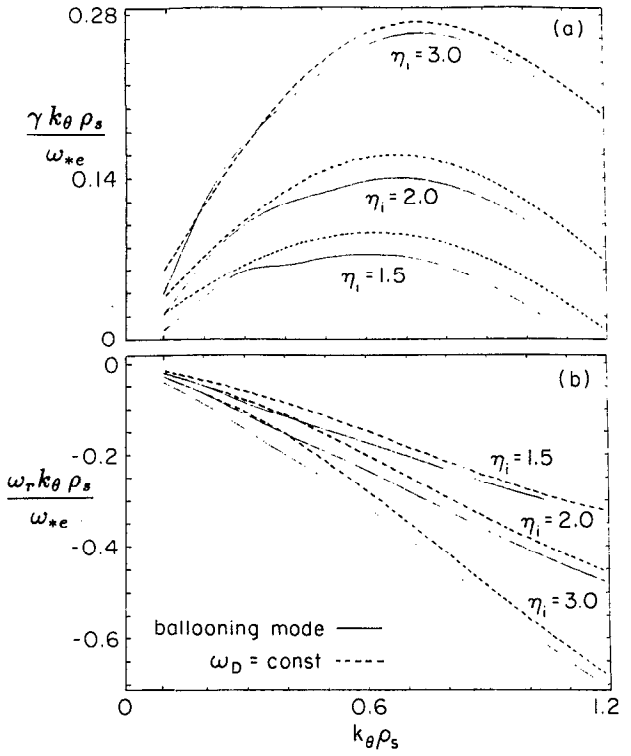

FIG. 3. (a) Normalized growth rate $\gamma\, k_\theta \rho_s/\omega_{*e}$ and (b) real frequency $\omega_r k_\theta \rho_s/\omega_{*e}$ vs $k_\theta \rho_s$ for $\eta_i = 1.5$, 2, and 3 when $T_e/T_i = 1$, $L_n/L_s = 0.1$, and $\epsilon_n = 0.2$. Dotted lines correspond to the quasitoroidal approximation, and the solid lines the general toroidal results with $q=2$ and $\hat{s} = L_n q/L_s \epsilon_n$.

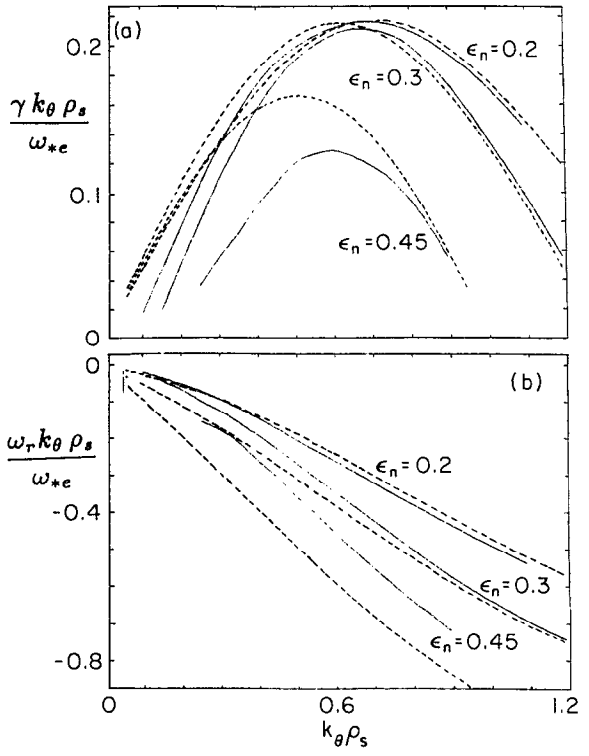

FIG. 4. (a) Normalized growth rate $\gamma\, k_\theta \rho_s/\omega_{*e}$ and (b) real frequency $\omega_r k_\theta \rho_s/\omega_{*e}$ vs $k_\theta \rho_s$ for $\epsilon_n = 0.2$, 0.3, and 0.45 when $T_e/T_i = 1$, $L_n/L_s = 0.1$, and $\eta_i = 2.5$. Dotted lines correspond to the quasitoroidal approximation, and the solid lines the general toroidal results with $q=1.5$ and $\hat{s} = L_n q/L_s \epsilon_n$.

given in Fig. 3 for different η_i values. Again, the differences between general toroidal (solid lines) and the quasitoroidal approximation (dotted lines) are limited. The maximum growth rates are found at $k_\theta \rho_s \sim 0.7$, indicating that small $k_\theta \rho_s$ expansion is not adequate and the full integral formalism is necessary for these parameters. The growth rate and real frequency for different ϵ_n values are given in Fig. 4 as function of $k_\theta \rho_s$. The maximum growth rates appear at $k_\theta \rho_s \sim 0.7$, just as it does in Fig. 3. Note that the real frequency and growth rate are normalized to $\omega_{*e}(k_\theta \rho_s)^{-1} = c_s/L_n$ in Figs. 3–5.

B. ϵ_n variation

In Fig. 5 the mode growth rate and real frequency are given as function of ϵ_n for different $k_\theta \rho_s$ values. Here, we consider only the ϵ_n effect coming from the toroidal curvature drift term ω_D, and $L_n/L_s = \hat{s}\epsilon_n/q = 0.1$ is fixed. In order to compare with the quasitoroidal model, $q=1.5$ is fixed, and $\hat{s}$ varies according to $L_n/L_s = \hat{s}\epsilon_n/q = 0.1$ in the general ballooning model (solid lines). It is easy to see that the mode real frequency increases significantly with the increasing of ϵ_n. The maximum growth rates occur around $\epsilon_n \simeq 0.2$, where the quasitoroidal approximation is good for general toroidal dynamics. Figure 5 can also be viewed as a normalized frequency and growth rate versus $\hat{s} \sim 1/\epsilon_n$. In this way it seems that mode coupling has a stronger destabilizing effect when the $\hat{s}$ value is higher, as expected. As an alternative, the results for fixed $\hat{s}=1.0$ and varying q, such that $L_n/L_s = \hat{s}\epsilon_n/q = 0.1$, are given (dashed line) when $k_\theta \rho_s = 0.5$. Such a choice does not change the result very much.

The mode growth rate and real frequency versus ϵ_n are given in Fig. 6 for fixed $\hat{s}=1.0$ and given q values (in Fig. 5, $\hat{s}$ or q varies when ϵ_n changes) for the general toroidal model. It is obtained that the mode real frequency increases up to $-1.3\omega_{*e}$ with the increasing $\epsilon_n \sim 0.5$, while the mode moves to the electron diamagnetic drift direction for $\epsilon_n \lesssim 0.06$. The maximum mode growth rate in this case is much higher than that in Fig. 5. This is reasonable, since in Fig. 5, $\hat{s}$ increases when ϵ_n decreases in order to keep L_n/L_s constant.

From Fig. 6 it is seen that the mode growth rate increases with q when other parameters are the same. The increase of q separates the favorable and the unfavorable magnetic curvature regions making the localization of the mode to the bad curvature region more complete, leading to higher mode growth rate and transport.

C. Shear variation

The shear variation effect is studied. The mode real frequency increases with shear increasing for $\hat{s} \lesssim 1$, then keeps constant for $\hat{s} > 1$. At the same time the mode growth rate increases with $\hat{s}$ increasing for $\hat{s} \lesssim 0.5$ then decreases for $\hat{s} \gtrsim 0.5$, as shown in Fig. 7. For the region $1 < \hat{s} < 2$ the growth rate decreases as $1/\hat{s}$. The growth rate obtained

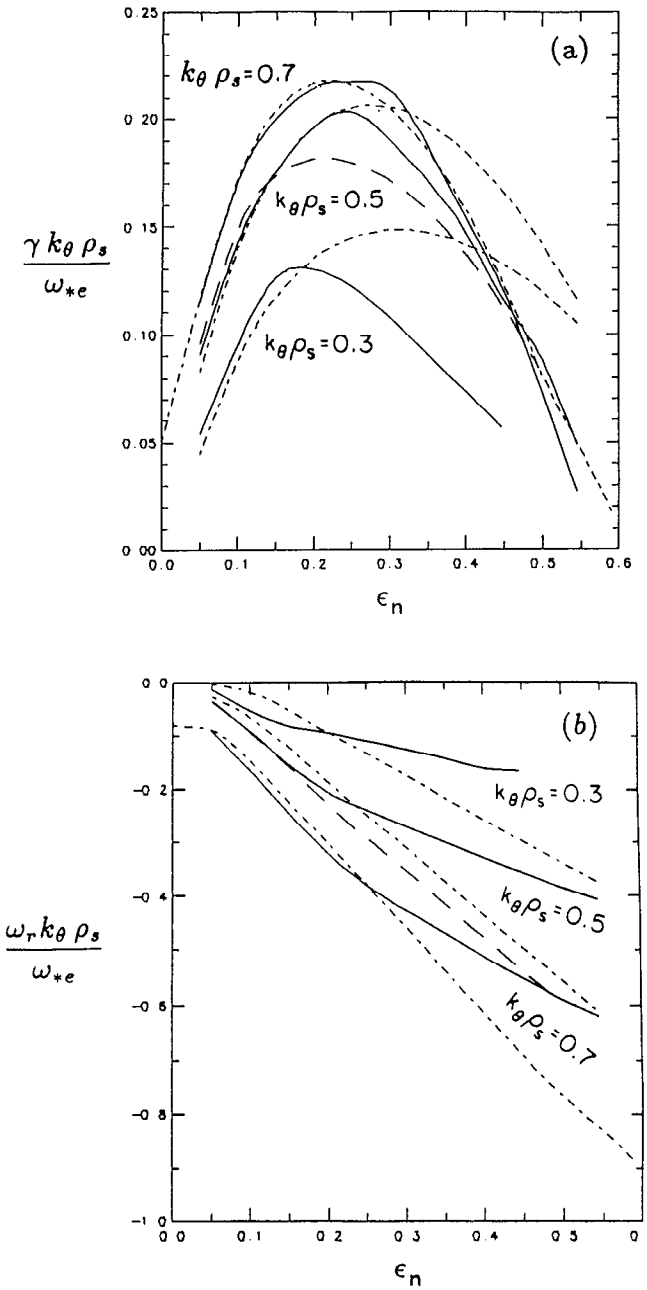

FIG. 5. (a) Normalized growth rate $\gamma k_\theta \rho_s/\omega_{*e}$ and (b) real frequency $\omega_r k_\theta \rho_s/\omega_{*e}$ vs ϵ_n for $k_\theta \rho_s = 0.3, 0.5$, and 0.7 when $\eta_i = 2.5$, $T_e/T_i = 1$, and $L_n/L_s = 0.1$. The dotted lines represent the quasitoroidal approximation, the solid lines the general toroidal results with $q = 1.5$, and the dashed line with $\hat{s} = 1.0$.

with the quasitoroidal approximation is higher than the general toroidal result for the parameters studied here. The quasitoroidal growth rate is basically constant while the growth rate obtained with the general toroidal equation decreases when $\hat{s}$ decreases for $\hat{s} \lesssim 0.5$, where the mode coupling destabilization effect is weak.

D. T_i variation at fixed T_e

The effect of increasing T_i at fixed T_e is studied in Fig. 8. The real frequency increases approximately linearly with T_i increasing. For $\epsilon_n = 0.15$ the real frequency becomes

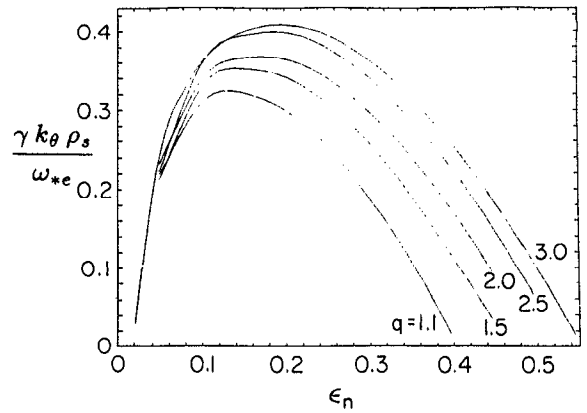

FIG. 6. Normalized growth rate γ/ω_{*e} vs ϵ_n for $q = 1.1$, 1.5, 2, 2.5, and 3 when $T_e/T_i = 1$, $\eta_i = 2.5$, $k_\theta \rho_s = 0.5$, and $\hat{s} = 1.0$. These are the general toroidal results.

positive (rotation in the electron direction) when T_i is low ($T_i \leqslant 0.25 T_e$). The mode growth rate has a maximum around $T_i \sim (0.5 - 1) T_e$. For $T_e/T_i \geqslant 2$ the mode width $\Delta\theta \gtrsim \pi/2$, so that the mode coupling destabilizing effect seems significant when shear is high enough (low ϵ_n for fixed q and L_n/L_s). For $T_e/T_i \leqslant 0.8$, $\epsilon_n = 0.15$, the mode width $\Delta\theta \leqslant \pi/3$ and the mode coupling destabilizing effect is weak [Fig. 8(c)]. This change of the mode width with T_e/T_i may explain the fact that the mode growth rate from the general toroidal calculation is higher than that from the quasitoroidal approximation for $T_e/T_i \geqslant 2$ while it is lower than that from the quasitoroidal for $T_e/T_i \leqslant 0.8$, when $\epsilon_n = 0.15$ in Fig. 8(a).

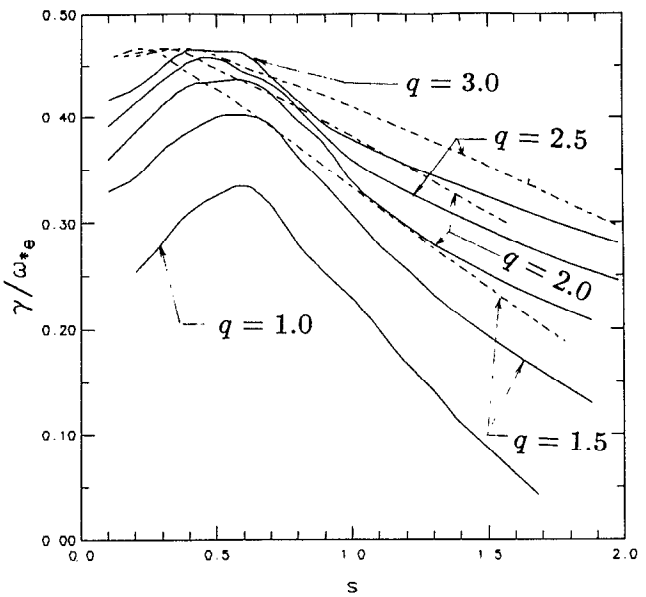

FIG. 7. Normalized growth rate γ/ω_{*e} vs $\hat{s}$ for $q = 1.5$, 2.0, and 2.5 when $\eta_i = 2.5$, $T_e/T_i = 1$, $k_\theta \rho_s = 0.5$, and $\epsilon_n = 0.25$. The solid lines represent the general toroidal results and the dotted lines the quasitoroidal approximation.

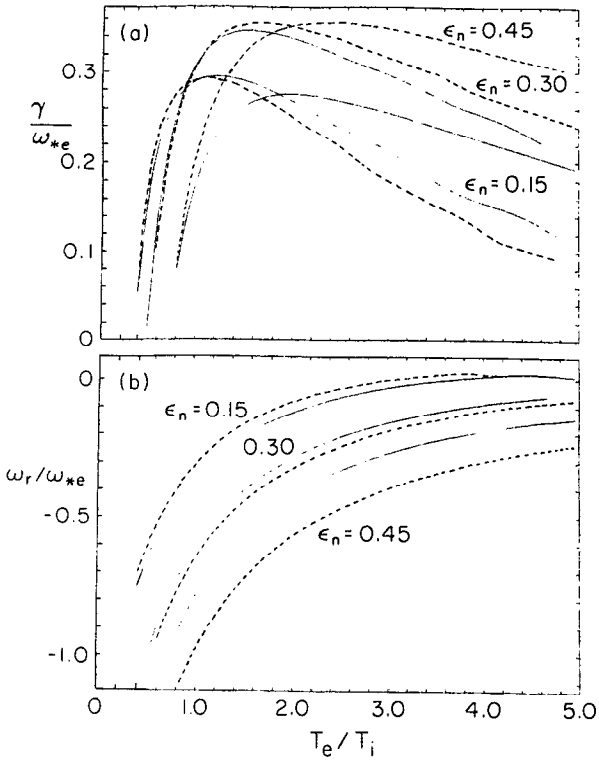

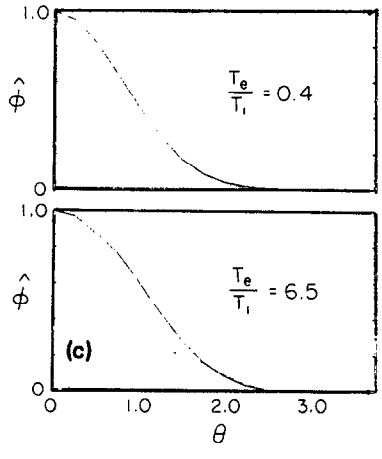

FIG. 8. (a) Normalized growth rate γ/ω_{*e} and (b) real frequency ω_r/ω_{*e} vs T_e/T_i (T_e = const) for various values of ϵ_n when $k_\theta\rho_s = 0.7$, $L_n/L_s = 0.1$, and $\eta_i = 2.5$. The dotted lines represent the quasitoroidal approximation and the solid lines the general toroidal results, where $q=1.5$ and $\hat{s} = L_n q/L_s\epsilon_n$ are used. (c) The eigenfunctions $\hat{\phi}(\theta)$ for $\epsilon_n = 0.15$.

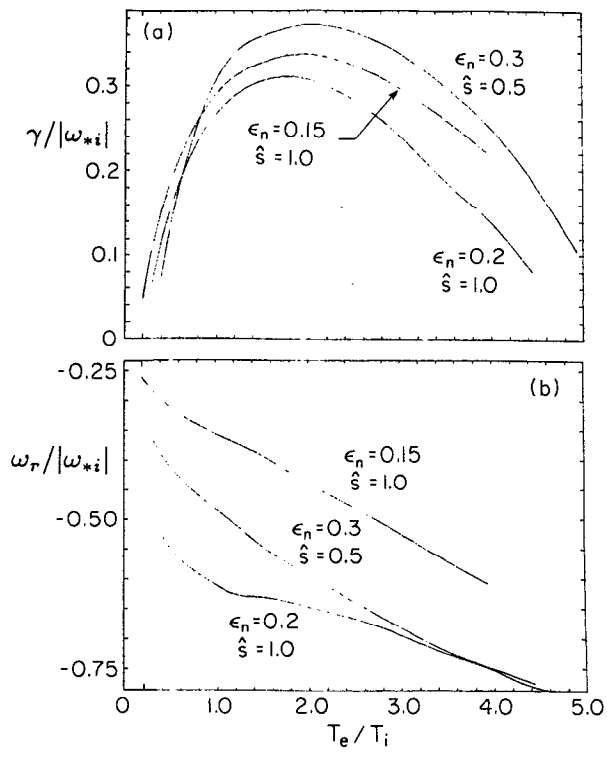

FIG. 9. (a) Normalized growth rate $\gamma/|\omega_{*i}|$ and (b) mode frequency $\omega_r/|\omega_{*i}|$ vs T_e/T_i (T_i = const) for $\eta_i = 2.5$, $k_\theta\rho_s = 0.70$, and $q=1.5$. These are the general toroidal results.

E. T_e variation at fixed T_i

The normalized mode frequency and growth rate (normalized to $-\omega_{*i} = \omega_{*e}T_i/T_e$) are given in Fig. 9 as a function of T_e/T_i to show the T_e effect when T_i is fixed. In contrast to Fig. 8, where the mode real frequency decreases when T_e/T_i increases, the mode frequency increases when T_e/T_i increases. The behavior of the growth rate is similar to that in Fig. 8, except that the maximum growth rate shifts to higher T_e/T_i and decreases much faster in Fig. 9. It seems necessary to distinguish T_e or T_i changing when T_e/T_i effect is considered. Especially, the behavior of the real frequency may be used to define the η_i-mode turbulence from the others in experiments.

F. Local kinetic model

The comparison between the general toroidal model and the local kinetic approximation is given in Fig. 10. For $k_\theta\rho_s \sim 1$ the results from these two models are very close, while the integral equation gives much higher growth rates when $k_\theta\rho_s \lesssim 0.5$.

G. Threshold η_i study

The threshold values $\eta_c(k_\theta\rho_s, q, \epsilon_n, \hat{s}, \tau)$ obtained with local approximation equation (22) (dotted lines) and general toroidal equation equation (11) (solid lines) are given in Fig. 11 as a function of $k_\theta\rho_s$ for $q=1$, 2, and 4. In the local case $k_\parallel = 1/qR$ is used. The threshold values obtained with the local approximation are higher than that obtained with the integral equation for $k_\theta\rho_s \lesssim 1$ and lower for $k_\theta\rho_s \gtrsim 1.4$. The minimum η_c, which gives the first $k_\theta\rho_s$ mode to go unstable, decreases and moves to the smaller $k_\theta\rho_s$ region as q increases. This is qualitatively in agreement with the experimental results that anomalous ion thermal conductivity χ_i decreases with the increasing of plasma current.[22] The q dependence of η_c is analyzed by Kim and Horton[25] within the local approximation.

The comparison between the general toroidal model [Eq. (11)] and the quasitoroidal model [Eq. (18)] cannot be made too precisely because there is one more parameter

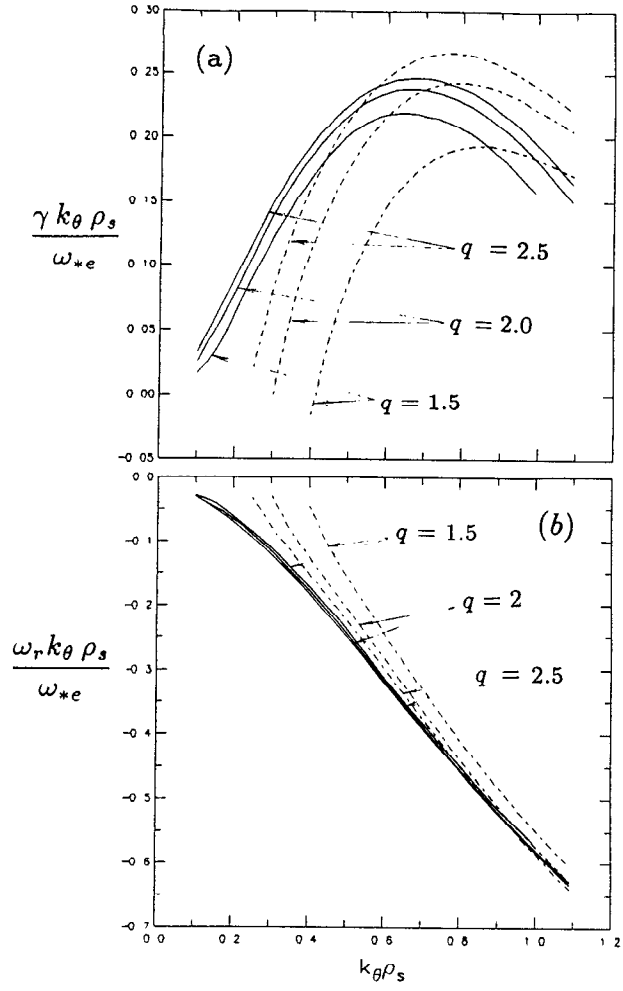

FIG. 10. (a) Normalized growth rate $\gamma\, k_\theta \rho_s/\omega_{*e}$ and (b) real frequency $\omega_r k_\theta \rho_s/\omega_{*e}$ vs $k_\theta \rho_s$ for $q=1.5$, 2.0, and 2.5 when $T_e/T_i = 1$, $\epsilon_n = 0.25$, $\hat{s}=0.6$, and $\eta_i = 2.5$. Dotted lines correspond to the local kinetic approximation where $k_\parallel = 1/qR$ is used, and the solid lines the general toroidal results.

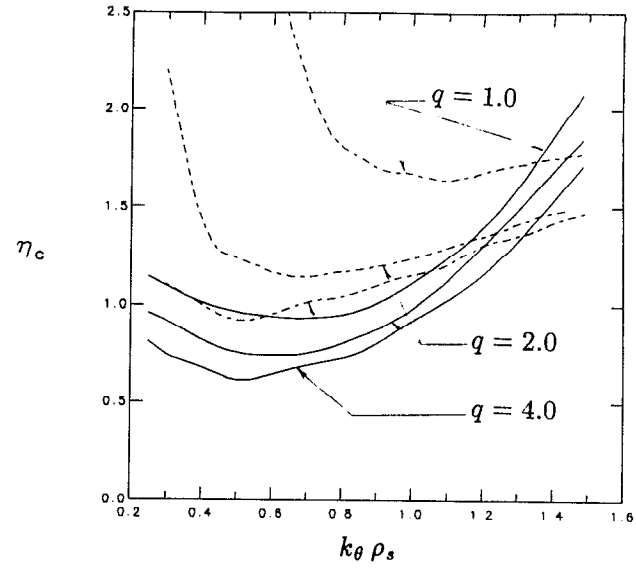

FIG. 11. Threshold value η_c vs $k_\theta \rho_s$ for $q=1$, 2, and 4. The dotted and solid lines are from the local and integral equations, respectively. The other parameters are $\epsilon_n = 0.2$, $\hat{s}=0.5$, and $\tau=1.0$.

that could be chosen freely in the former than in the latter. Generally speaking, the quasitoroidal approximation overestimates the driving force of curvature and magnetic gradient drifts (by taking $\theta=0$), and gives higher growth rate. However, mode coupling that is considered only in the general toroidal model has a strong destabilizing effect when the mode width $\Delta\theta$ is large enough and shear is high ($\hat{s} \gtrsim 1.0$). In such cases, the growth rate given by the toroidal model is about 10%–20% higher than that given by the quasitoroidal approximation. It has never appeared that the mode growth rate obtained from the toroidal equation is much higher than the growth rate obtained from the quasitoroidal approximation.

IV. REMARKS AND DISCUSSIONS

A new integral equation describing the linear dynamics of low-frequency perturbations such as the η_i mode in toroidal geometry is developed. The integral equation takes into account the ion drift motion due to the curvature and magnetic gradient, the effect of finite Larmor radius, and the arbitrary ratio of $k_\parallel v_t/\omega_D$. Ion bounce motion is neglected, and the electrons are taken as adiabatic, for simplicity. Under these conditions the integral equation is the most general equation.[8] In addition, the new formalism of the integral equation has some characteristics that allow the equation to be solved within reasonable computer time ($\sim$3 min/eigenvalue on the CRAY-2).

The equation is solved for a wide range of tokamak plasma parameters without further approximation. It can be concluded from the calculations that the real frequency and growth rate of the η_i mode in toroidal geometry are significantly different from the sheared slab η_i mode. Toroidicity effects must be taken into account, in an effort to connect theoretical results of the η_i-mode analysis with experimental observations in tokamaks. The numerical results presented in this work can be used to check the validity of various approximation approaches, and may be compared with experimental observations. A numerical table of the complex eigenvalue over the parameter variation considered is being made available on a public domain file or on a disk available upon request.

By using the ballooning mode representation the mode coupling introduced due to the toroidal feature of the equilibrium magnetic configuration is taken into account. It is shown that the mode coupling has a strong destabilizing effect especially when mode width $\Delta\theta \geqslant \pi/2$ and magnetic shear $\hat{s} \geqslant 1$ due to the geodesic curvature effect from $\hat{s}\theta \sin\theta$ term in Eq. (5).

It is worth mentioning that the real frequency of the mode for $\epsilon_n = 0.4$ is about one order of magnitude higher than the corresponding sheared slab mode frequency [see Fig. 1(b)]. The low theoretical mode frequencies of previous ITG models are claimed to be too low to explain the ion feature observed on TEXT[6] (Texas Experimental Tokamak) drift wave fluctuation spectrum.[26] The increase in

the mode frequency from the toroidal effect is in the right direction, at least in this respect.

In addition, it is claimed that ion energy transport coefficients obtained from kinetic η_i-mode quasilinear theories are lower than experimental measurements.[7,11] It is shown in this work that the η_i-mode growth rate in toroidal geometry is much higher than in the sheared slab, for example, the growth rate for $\epsilon_n = 0.4$ is about three times the value of the sheared slab mode when $\eta_i = 3.0$ [see Fig. 1(a)]. At the same time the mode width in x space for the toroidal geometry is about twice the value of the sheared slab mode width (see Fig. 2). This increase of $\gamma(\Delta x)^2$ is in the direction for solving the discrepancy between the η_i-mode theory and the experimental observations concerning the anomalous ion energy transport. The mode growth rate decreases with ϵ_n increasing for $\epsilon_n \gtrsim 0.2$. This qualitatively agrees with the confinement improvement in H-mode discharges, which have a rather large value of L_n. Detailed calculation using experimental data and comparison with observed results are underway, and will be published separately. It is also straightforward to couple trapped electron and impurity effects into Eq. (11), and such a work is in progress.

Maxwellian velocity distribution is used in this work. The treatment of non-Maxwellian equilibrium distributions is limited by the requirement that the velocity integrals need to be carried out analytically in the present approach, which leaves only the time integral to be performed numerically. However, distribution functions of the bi-Maxwellian form or Maxwellians with an equilibrium drift velocity can be integrated analytically, so that the present approach can be extended to such cases, although the formulas become cumbersome. The local stability analysis for the bi-Maxwellian has recently been completed by Kim *et al.*,[27] where it is shown that for the toroidal modes the η_c remains near $\frac{2}{3}$ for $T_\perp \neq T_\parallel$.

ACKNOWLEDGMENTS

The authors would like to thank Dr. Y. Z. Zhang for helpful discussions.

This work was supported by U.S. Department of Energy Contract No. DE-FG05-80ET-53088.

[1]M. Greenwald, D. Q. Winn, S. Milora, R. Parker, and S. Wolfe, Phys. Rev. Lett. **53**, 352 (1984)

[2]F. X. Sölder, E. R. Müller, F. Wagner, H. S. Bosch, A. Eberhagen, H. V. Fahrbach, G. Fussmann, O. Ghre, K. Gentle, J. Gernhardt, O. Gruber, W. Herrmann, G. Janeschitz, M. Kornherr, K. Krieger, H. M. Mayer, K. McCormick, H. D. Murmann, J. Neuhauser, R. Nolte, W. Poschenreider, H. Röhr, H.-H. Steuer, U. Stroth, N. Tsois, and H. Verbeek, Phys. Rev. Lett. **61**, 1105 (1988).

[3]R. J. Fonk, R. Howell, K. Jaehnig, L. Roquemore, G. Schilling, S. Scott, M. C. Zarnstorff, C. Bush, R. Goldston, H. Hsuan, D. Johnson, A. Ramsey, J. Schivell, and H. Towner, Phys. Rev. Lett. **63**, 520 (1989).

[4]S. D. Scott, P. H. Diamond, R. J. Fonck, R. B. Howell, K. P. Jahnig, G. Schilling, E. J. Synakowski, M. C. Zarnstorff, C. E. Bush, E. Fredrickson, K. W. Hill, A. C. Janos, D. K. Mansfield, D. K. Owens, H. Park, G. Pautasso, A. T. Ramsey, J. Schivell, G. D. Tait, W. M. Tang, and G. Taylor, Phys. Rev. Lett. **64**, 531 (1990).

[5]D. L. Brower, W. A. Peebles, S. K. Kim, N. C. Luhmann, W. M. Tang, and P. E. Phillips, Phys. Rev. Lett. **59**, 48 (1987).

[6]D. L. Brower, M. H. Redi, W. M. Tang, R. V. Bravenec, R. D. Durst. S. P. Fan, Y. X. He, S. K. Kim, N. C. Luhmann, Jr., S. C. McColl, A. G. Meigs, M. Nagatsu, A. Ouroua, W. A. Peebles, P. E. Phillips, T. L. Rhodes, B. Richards, C. P. Ritz, W. L. Rowan, and A. J. Wootton, Nucl. Fusion **29**, 1247 (1989).

[7]W. Horton, D. Lindberg, J.-Y. Kim, J. Q. Dong, G. W. Hammett, S. D. Scott, M. C. Zarnstorff, and S. Hamaguchi, Phys. Fluids B **4**, 953 (1992).

[8]F. Romanelli, Phys. Fluids B **1**, 1018 (1989).

[9]T. S. Hahm and W. M. Tang, Phys. Fluids B **1**, 1185 (1989).

[10]J. Q. Dong, P. N. Guzdar, and Y. C. Lee, Phys. Fluids **30**, 2694 (1987).

[11]M. Kotschenreuther, H. L. Berk, R. Denton, S. Hamaguchi, W. Horton, C.-B. Kim, M. Lebrun, P. Lyster, S. Mahajan, W. H. Miner, P. J. Morrison, D. Ross, T. Tajima, J. B. Taylor, P. M. Valanju, H. V. Wong, S. Y. Xiao, and Y.-Z. Zhang, in *Plasma Physics and Controlled Nuclear Fusion Research, 1990* (IAEA, Vienna, 1991), Vol. II, p. 361.

[12]W. Horton, B.-G. Hong, and W. M. Tang, Phys. Fluids **31**, 2971 (1988).

[13]S. Hamaguchi and W. Horton, Phys. Fluids B **2**, 3040 (1990).

[14]L. Chen, S. Briguglio, and F. Romanelli, Phys. Fluids B **3**, 611 (1991).

[15]R. R. Dominguez and M. N. Rosenbluth, Nucl. Fusion **29**, 844 (1989).

[16]J. Y. Kim and W. Horton, Phys. Fluids B **3**, 1167 (1991).

[17]C. Z. Cheng and K. T. Tsang, Nucl. Fusion **21**, 643 (1981).

[18]P. N. Guzdar, L. Chen, W. M. Tang, and P. H. Rutherford, Phys. Fluids **26**, 673 (1983).

[19]X. Q. Xu and M. N. Rosenbluth, Phys. Fluids B **3**, 627 (1991).

[20]G. Rewoldt and W. M. Tang, Phys. Fluids B **2**, 318 (1990).

[21]Y. C. Lee, J. Van Dam, and A. Glasser, in *Proceedings of the Finite Beta Theory Workshop 1977* (U.S. Department of Energy, Washington, DC, 1977), pp. 55, 93.

[22]S. D. Scott, C. W. Barnes, L. R. Grisham, G. W. Hammett, W. W. Heidbrink, D. W. Johnson, Y. Kusama, M. C. Zarnstorff, S. J. Zweben, M. G. Bell, M. Bitter, R. Boivin, R. Budny, C. E. Bush, A. Cavallo, C. Z. Cheng, V. Decaux, P. C. Efthimion, R. J. Fonck, E. D. Fredrickson, R. J. Goldston, B. Grek, R. J. Hawryluk, K. W. Hill, H. Hsuan, A. C. Janos, D. L. Jassby, F. C. Jobes, L. C. Johnson, R. Kaita, S. M. Kaye, P. H. LaMarche, B. LeBlanc, D. K. Mansfield, J. McCauley, D. C. McCune, K. M. McGuire, S. S. Medley, D. Mueller, J. Murphy, H. Mynick, Y. Nagayama, D. K. Owens, H. K. Park, R. Perkins, S. Pitcher, A. T. Ramsey, A. L. Roquemore, J. Schivell, G. L. Schmidt, W. Stodiek, B. C. Stratton, E. J. Synakowski, W. M. Tang, G. Taylor, H. H. Towner, S. Von Goeler, R. E. Waltz, R. M. Wieland, M. Williams, and K. M. Young, in *Plasma Physics and Controlled Nuclear Fusion Research* (IAEA, Vienna, 1991), Vol. I, p. 235.

[23]R. Courant and D. Hilbert, *Methods of Mathematical Physics* (Interscience, New York, 1953), Vol. 1, p. 112.

[24]B. G. Hong and W. Horton, Phys. Fluids B **2**, 978 (1990).

[25]J. Y. Kim and W. Horton (private communication).

[26]W. A. Peebles, D. L. Brower, R. Philipona, K. Burrell, R. Bravenec, E. J. Doyle, R. Groebner, N. C. Luhmann, Jr., H. Matsumoto, C. Retig, B. A. Smith, C. X. Yu, R. P. Seraydarian, Z. M. Zhang, and the DIII-D/TEXT Research Groups, N. Bretz, A. Cavallo, R. J. Fonck, T. S. Hahm, E. Mazzucato, R. Nazikian, S. F. Paul, G. Rewoldt, D. R. Roberts, W. M. Tang, G. Taylor, and the TFTR Research Group, in *Plasma Physics and Controlled Nuclear Fusion Research* (IAEA, Vienna, 1991), Vol. I, p. 589.

[27]J. Y. Kim, W. Horton, D. I. Choi, S. Migliuolo, and B. Coppi, Phys. Fluids B **4**, 152 (1992).